Article Identifier
DOI: 10.22032/dbt.58852
URN: urn:nbn:de:gbv:ilm1-2023isc-036:6

Directed Energy Deposition-Arc (DED-Arc) and Numerical Welding Simulation as a method to determine the homogeneity

Jan Reimann, Maximilian Rohe, Alexander Rauch, Jörg Hildebrand, Jean Pierre Bergmann

Production Technology Group, Technische Universität Ilmenau, D-98693 Ilmenau, Germany

ABSTRACT

This research presents a hybrid approach to for the prediction of the homogeneity of mechanical properties in 3D metal parts manufactured using directed energy deposition-arc (DED-Arc). DED-Arc is an additive manufacturing process which can offer a cost-effective way to manufacture 3D metal parts, due to high deposition rate of up to 8 kg/h. Regression equations developed in a previous study were used to predict the mechanical properties of a wall structure using only the cooling time $t_{8/5}$ calculated in a numerical welding simulation. The new approach in this research paper contains the prediction of the homogeneity of the mechanical properties, especially hardness, in 3D metal parts, which can vary due to localized changes in $t_{8/5}$ cooling time provoked by specific geometrical features or general changes in dimensions. In this study a method for the calculation of the hardness distribution on additively manufactured parts was developed and shown.

Index Terms – Directed Energy Deposition – Arc; DED-Arc; WAAM; wire arc additive manufacturing; Wire arc; GMAW; Gas metal arc welding; Wire-based; Arc; Additive manufacturing; numerical welding simulation.

INTRODUCTION

The market for additive manufacturing processes regarding metallic parts is growing continuously, with a 41.9 % growth rate of in 2018 [1]. Processes for the manufacturing of metal includes different technologies, such as Powder Bed Fusion (PBF) or Direct Energy Deposition (DED) [2]. The differentiation between these processes are the form of the deployed

material (powder or wire) and the used power source (electron beam, laser or electric arc) [3]. These differences result in varying build-up rates, productivity, near net shape, surface roughness or waviness of the additively manufactured part using different additive manufacturing process.

Directed Energy Deposition – Arc (DED-Arc) can utilize Tungsten Inert Gas Welding (TIG), Gas Metal Arc Welding (GMAW) and plasma processes during additive manufacturing. These three processes have in common that a layer-by-layer approach is utilized while feeding and melting a wire-shaped filler material to deposit the welding layers. The additive and layer wise approach using DED-Arc enables the application in lightweight constructions due to the possibility of the generation of undercuts, cavities. Furthermore any cooling channels running in the component which cannot be produced or can only be produced to a limited extent using conventional methods (e.g. [4,5]) are made possible by additive manufacturing. The GMAW process, in particular, is characterized as a cost-effective and robust process technology for additive manufacturing. The utilization of the GMAW process in DED-Arc can achieve deposition rates of up to 8 kg/h, depending on the material and component geometry [6–9].

There are generally no restrictions regarding the workspace size, due to the localized inert gas coverage. While the coaxial fed filler material enables the DED-Arc process to be independent of the welding direction. Therefore, the handling system is the main limitation of the buildable volume. Thus large scale components can be produced using the DED-Arc process [7,10]. Though, the dimensional accuracy or surface quality is limited due to comparatively large melt pool sizes. Therefore subtractive post processing of the manufactured parts, at least for functional surfaces, is necessary to meet the required tolerances [6,11,12]. Figure 1 shows an example of a DED-Arc process chain.

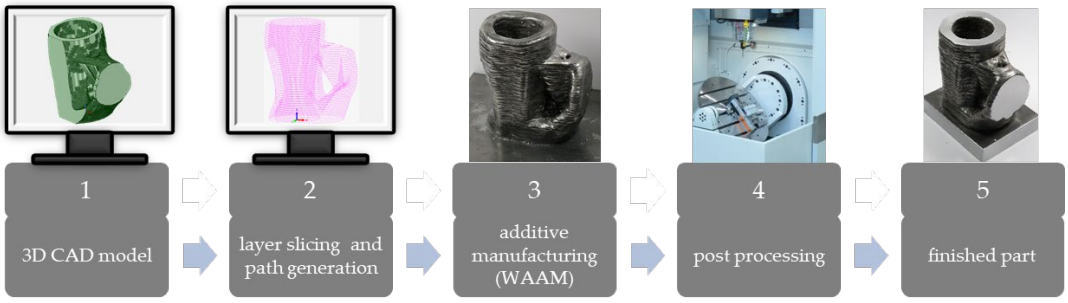

Figure 1. Process chain of additive manufacturing using DED-Arc according to [11]

The application of additive manufacturing of metallic components is manifold. Lately it was used to produce aerospace parts or for high-performance applications in the energy sector. Due

to these high performance and high temperature applications titanium alloys [13,14] and nickel-base alloys [15,16] gained increasing interest. Thus cost efficient production systems were developed [17]. These systems are capable of high deposition rates, which increases the accessible of additive manufacturing for enterprises in fields such as architecture or construction engineering. Moreover complex 3D structures are possible for many industries, due to the high degree of freedom [18–21]. The potential of this technology is demonstrated in recent scientific literature with a variety of investigations on a plethora of materials such as aluminum [22,23], hot work tool steel [24] high-alloyed steel [25,26] and low-alloyed steel [27–30], or in addition to the mentioned titanium and nickel base alloys.

The DED-Arc process, characterized by intense and repeated energy input, induces a range of intricate effects including complex thermal profiles, residual stress, and deformations. Finite element methods present an opportunity to examine mitigation strategies for thermo-mechanical problems induced by the DED-Arc process.

These methods enable the investigation of recurring thermal cycles, distortion, and the impact of heat sources on thermal behavior. Consequently, the intricate interplay between these factors can yield a more comprehensive understanding of the relationship between thermal cycles, mechanical properties, and transient data throughout the simulated part [31–36,36–39].

In their study, Pu et al. conducted tests on various heat source models to evaluate their effectiveness in predicting residual stress and deformation in butt-welded joints. The results revealed that the moving heat source model closely aligned with the measured welding deformation, whereas the instantaneous heat source models exhibited poor accuracy in predicting deformation [40]. Similarly, Rikken et al. demonstrated the value of data fusion by integrating simulation and experimental data to gain new insights into residual stress in welding applications. Through a comprehensive approach encompassing detailed material research, thermal analysis, and robust mechanical simulation of the welding process, they successfully achieved accurate predictions of the through-thickness residual stress state [46].

In the introduction, it was identified that there is a lack of research that regarding the prediction of mechanical properties and homogeneity for DED-Arc processes in combination with the utilization of numerical simulation. However, an alternative approach that can address these limitations is data fusion by using regression equations comprised of experimental data and $t_{8/5}$ cooling time. Therefore, the primary objective of this investigation is to establish a foundation for employing data fusion for the prediction of the homogeneity of materials properties in DED-Arc processes. By integrating transient thermal welding simulation data with experimental datasets, data fusion techniques can be utilized to enhance the useable data from both datasets.

This approach allows a comprehensive understanding of the additive manufacturing process, particularly focusing on the $t_{8/5}$ cooling times, which play a crucial role in predicting mechanical properties. Regression equations can be developed based on this dataset using a relatively small experimental data set as a starting point. The significance of data fusion lies in its potential to enable predictions and analysis of mechanical properties for complex three-dimensional structures that may not be feasible to obtain physical samples for tensile or hardness tests. By incorporating validated numerical simulations into the data fusion process, it becomes possible to extract insights and accurately predict the properties of intricate structures, overcoming the limitations of traditional testing methods.

Overall, this study aims to explore the novel application of data fusion in DED-Arc processes, leveraging the integration of numerical simulations and experimental data to enhance the understanding and prediction of mechanical properties for a wide range of complex structures.

MATERIALS AND METHODS

Materials and additive manufacturing

The process of generating cuboid structure involved the use of a GMAW welding power source called “EWM Titan XQ 500 puls D EX W”. The power source utilized the "coldArc" technology, which is an energy reduced short arc process. To ensure consistent torch movement, a 6-axis industrial robot known as the "Kuka KR150-2" was utilized. The cuboid was created using a low-alloyed solid wire electrode called DIN EN ISO 14341-A-G4Si1 (ER70 S-6), while the base material (substrate) had a thickness of 10 mm and was made of S355J2+N. The chemical compositions of the welding wire and base material are provided in Table 1.

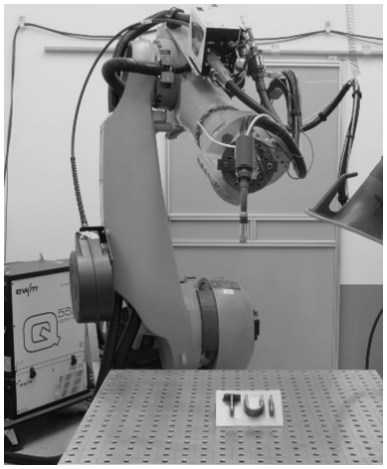

Figure 2. Experimental setup

Table 1. Chemical composition of substrate [41] and welding wire [42] (%).

	Material	Fe_{max}	C_{max}	Si_{max}	Mn_{max}	Cu_{max}
welding wire	G4Si1/SG3 (1.5130)	balance	0.07	1.00	1.64	0.05
base material	S355J2 + N (1.0570)	balance	0.20	0.55	1.60	0.55

The cuboid was generated using a linear welding strategy with parallel welding beads, which were processed with an alternating welding path. The cuboid was welded with 9 welding beads width and 20 layers, which resulted in 100 mm x 34.1 mm x 57.2 mm (Figure 3). In order to measure the time-temperature cycle during the additive manufacturing process, type C thermocouples were inserted into the molten metal. These thermocouples provided transient measurements.

Preliminary parameter studies [18] were conducted to identify suitable parameter sets for the additive manufacturing of G4Si1. In Reimann et. al. three parameter sets were developed, which consisted of different energy inputs per unit length: 4 kJ/cm, 6 kJ/cm, and 8 kJ/cm. Each energy input was associated with a specific wall thickness and different weld path planning [43]. The weld path planning included options such as one, two, or three adjacent rows, as well as a meandering weld path. The adjacent rows and meandering weld path were welded with a 35% overlap. According to these results the parameter set with 4 kJ/cm was uses to manufacture the cuboid with adjacent welding paths.

A complete presentation and discussion of the results were discussed at length in a previous study by Reimann et. al. [43]. The regression equations in Reimann et. al. [43] were used to determine the homogeneity regarding the hardness of the additively manufactured cuboid.

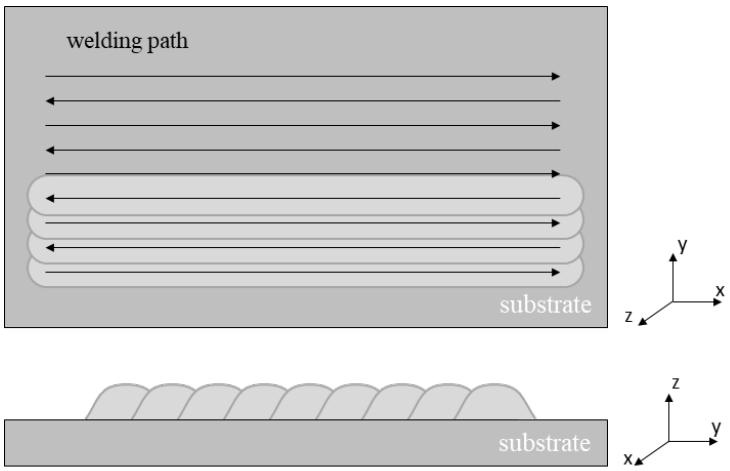

Figure 3. Schematic welding path planning

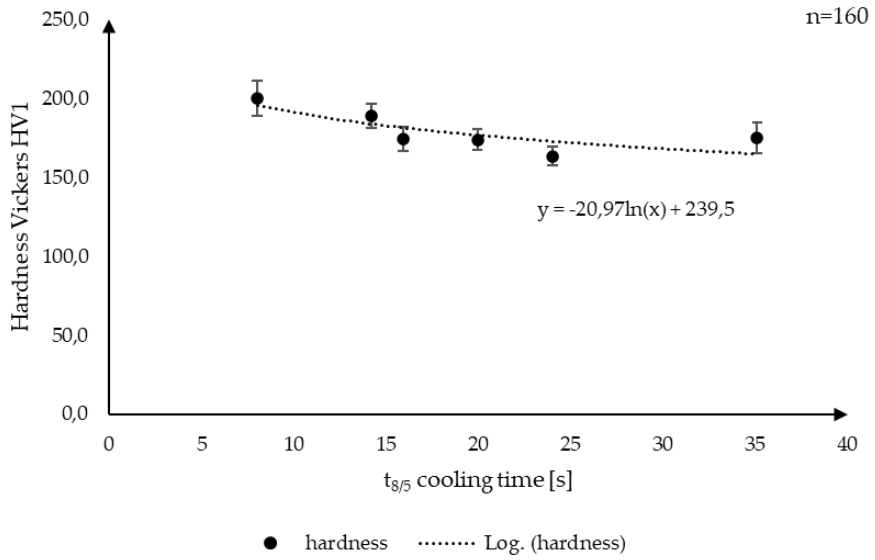

Figure 4. Hardness as a function of $t_{8/5}$ cooling time from measured data [43]

Numerical simulation

The numerical welding simulations were carried out in the MSC Software Simufact Welding 2021.1 with two different geometries using the 4 kJ/cm cuboid set, which was welded, tested, and used to create the simulation model and determine the homogeneity of the additively manufactured parts. The numerical welding simulation was carried out for the cuboid structure with 100 x 34,1 x 50 mm (Figure 6). The material model for the ER-70s in Simufact welding was used in the numerical welding simulation. This is a standard material in the materials library and was calculated using JMatPro, a simulation software which is particularly aimed at the calculation of multi-component alloys used in industrial practice. The $t_{8/5}$ cooling time for all simulations was derived in layer 17. As Henckell et al. stated, the quasi-static part starts in layer 20 for wall structures made of G4Si1 [44], therefore it is reasonable to assume a quasi-static behavior after 153 weld beads In one welding layer there is more than one passthrough of the temperature field of 800°C-500°C. The used $t_{8/5}$ cooling time is the last passthrough with a complete austenitization, as in the experiments. In the study conducted by Reimann et al. [43] different mesh size convergences were analyzed regarding their differences in $t_{8/5}$ cooling time. These different mesh sizes represented models with four, two and one elements per welded layer and exhibited a similar trend, albeit with time shifts. These shifts are a result of the temperature constraint, where the welding process dynamically initiates when all elements reach a temperature below 100 °C. The varying number of elements leads to different initiation times.

The $t_{8/5}$ cooling times were measured as 7.867 s for the 0.5 mm mesh size, 7.238 s for the 1 mm mesh size, and 7.552 s for the 2 mm mesh size. This indicates a small difference of 4% between the 2.0mm mesh size and the 0.5 mm mesh size, as well as a 4% difference between the 1 mm and 2 mm mesh sizes. Consequently, the 2 mm mesh size was selected to ensure shorter simulation times in Reimann et. al. [43]. Due to the previous results regarding the mesh convergence analysis either four, two or even one element per welded layer are suitable for an accurate simulation. In this research paper a mesh with two elements per welded layer was used, which results in a 1.43 mm mesh size. For additional details on the boundary conditions, please refer to Table 2. By utilizing the simulated $t_{8/5}$ cooling times, it is possible to calculate the corresponding mechanical properties using the regression equations derived from the study. This approach allows for the manual prediction of mechanical properties for a specific three-dimensional workpiece prior to its manufacturing or testing. Thus, it is possible to derive the homogeneity by calculating the resulting properties regarding varying cooling times across one or more welding layers. The simulation, coupled with the regression equations, provides a valuable tool for estimating the mechanical characteristics of the workpiece based on the known cooling time. This predictive capability can aid in making informed decisions and optimizing the manufacturing process without the need for physical testing of every individual workpiece.

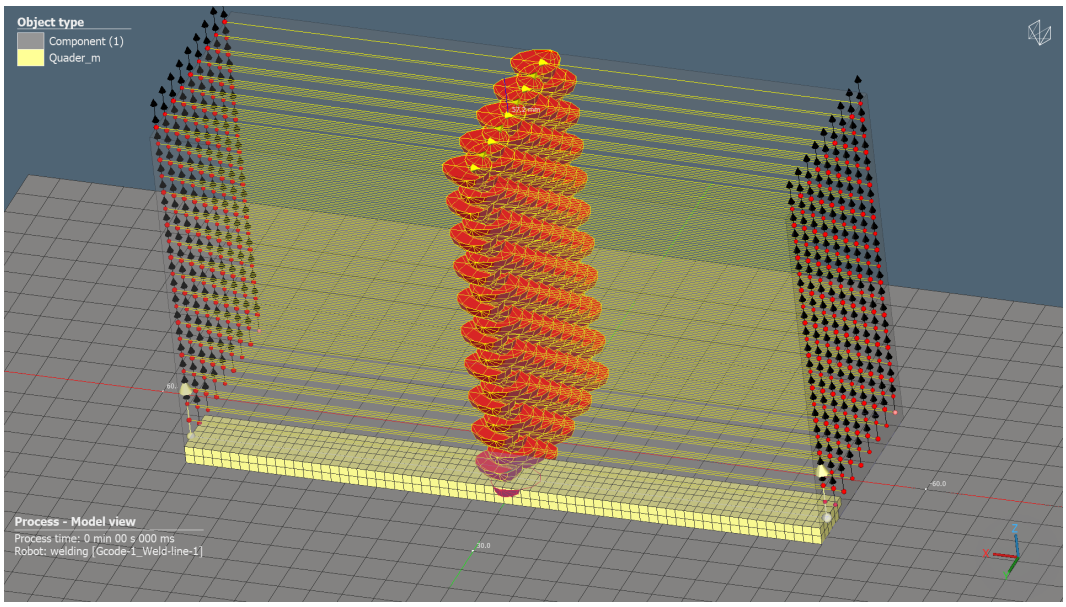

Figure 5. mesh with two elements per welding layer, shown in welding bead 9 in the first welding layer of the cuboid

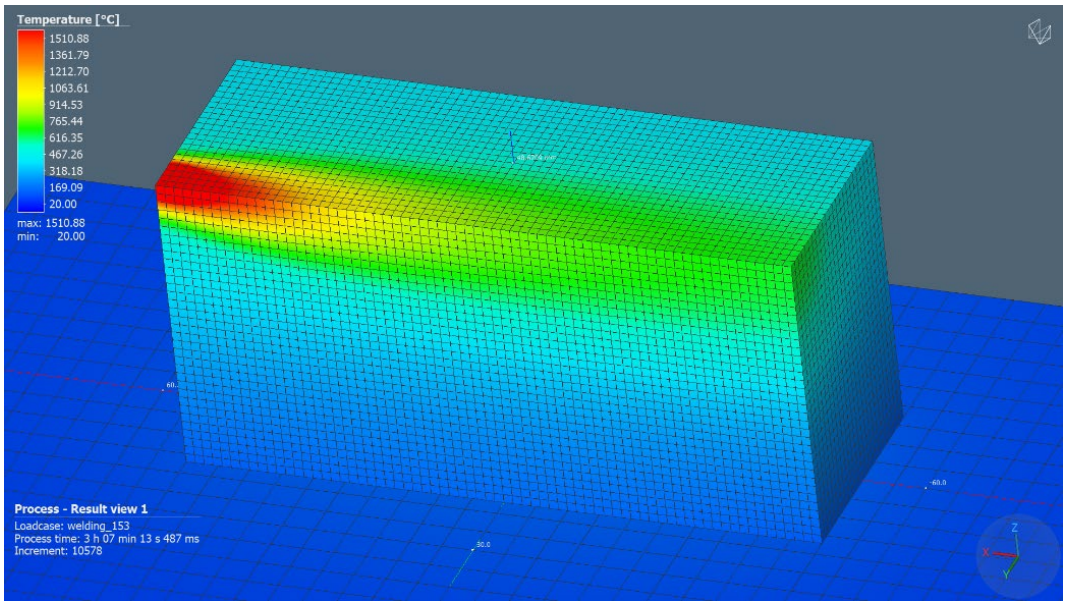

Figure 6. Meshed cuboid for numerical welding simulation

Table 2. Boundary conditions for numerical welding simulation

Boundary condition	**4 kJ/cm cuboid**
Mesh elements	hexahedral
Mesh size x/y/z-direction	2 mm
Heat source	Goldak
Heat source front length a_f	2.5 mm
Heat source rear length a_r	5.0 mm
Heat source width b	3.45 mm
Heat source depth d	3.0 mm
Heat source power	2650 W
Heat source movement speed	0.4 m/min
Convective heat transfer coefficient h	30 W/(m²*K)
Contact heat transfer coefficient a	1200 W/(m²*K)
Emission coefficient ε	0.8
Interpass temperature	100 °C

RESULTS AND DISCUSSIONS

Numerical simulation – $t_{8/5}$ cooling time and calculated hardness

In order to determine the homogeneity of an additively manufactured part using a structural welding simulation, particles as measurement points are needed to extract the necessary data. In Figure 8 the result view of the numerical simulation of the cuboid (Table 2) is shown. Three rows of particles were generated starting at the right most corner with an x distance of 0 mm. Row 1 is at the edge of the simulated cuboid with a y-distance to the middle of 17.05 mm. The second row has a y-distance of 8.525 mm and the third row is at 0 mm. Each particle has a spacing of 1 mm in x direction, starting at 0 mm and ending at 50 mm, which is the middle of the simulated part. The welding direction can be deduced from Figure 8, the start of the last welding bead of the measured layer is positioned at an x-distance of 0 mm and an y-distance of 17.05 mm. The heat source is moving in the positive x direction.

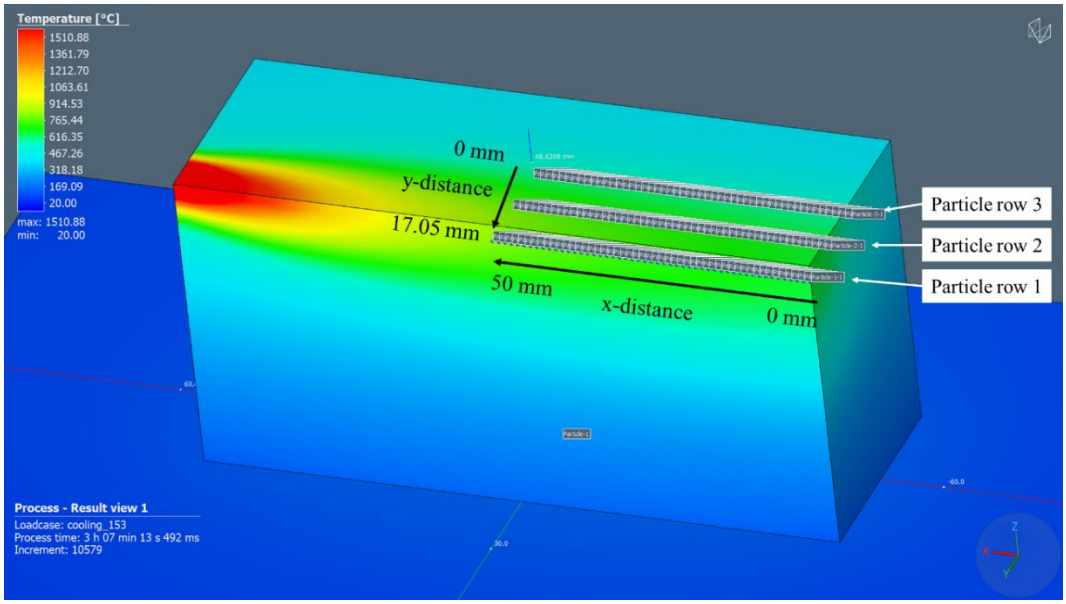

Figure 7. result view numerical welding simulation

The simulated $t_{8/5}$ cooling times for the three rows can be seen in Figure 9 to Figure 11 with their respective calculated hardness. The values for the hardness were calculated using the formula developed in the previous research (Figure 4). The $t_{8/5}$ cooling time for row 1(Figure 9) is constantly rising in travel direction of the moving heat source, which is as pronounced due to the position of the row. It is located directly at the edge of the manufactured part; therefore, the conductive heat transfer is greatly obstructed in the positive y direction. The rising $t_{8/5}$ cooling times result in a decreased hardness. The first five data points show a $t_{8/5}$ cooling which

is 10 s lower than the other measured values, this can be a result of the starting location of the welding, due to the relatively low interpass temperature of 100 °C.

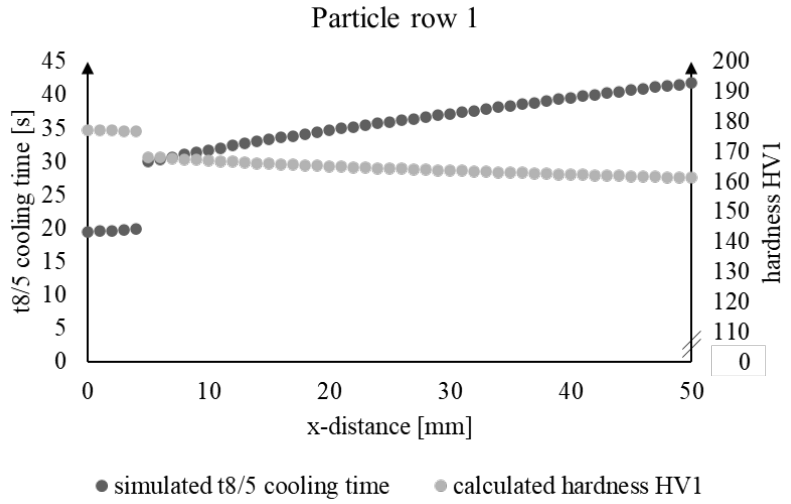

Figure 8. simulated $t_{8/5}$ cooling time and calculated hardness particle row 1

The simulated values of the $t_{8/5}$ cooling time and therefore the calculated hardness of row 2 (Figure 10) show a different progression in x direction than row 1. Most noticeably the is no starting section with $t_{8/5}$ cooling times that are way lower than in the later particles, this is a result of a different interpass temperature, which is 1000 °C between welding beads in the same layer. Only between the distinct layers the interpass temperature is at 100 °C. The $t_{8/5}$ cooling time is still slightly increasing over the course of the traveling heat source, which in turn results in a lower hardness.

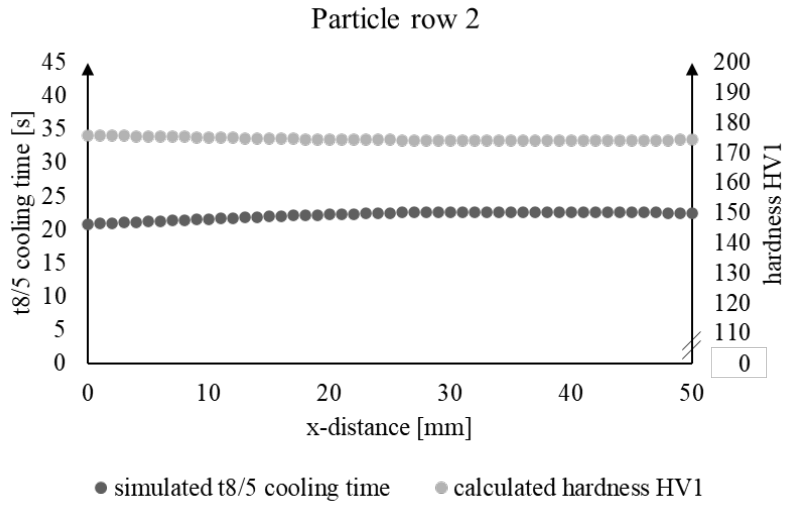

Figure 9. simulated $t_{8/5}$ cooling time and calculated hardness particle row 2

The third row of particles does not show a continuous path for the $t_{8/5}$ cooling time, which jumps at a x distance of 35 mm approx. 25 s to approx. 9 s. This is probably be a result of a discontinuity in the mesh for the simulation, a result of particle position or an edge case due to the time step size. In either case this is an issue which should be investigated further in mesh and time step studies to prevent such a behavior and to enhance the accuracy of the numerical simulation. Moreover, it is important to determine the influence of the position of particles in regard to their position on mesh knots or in between them. In general a rising $t_{8/5}$ cooling time can be observed for this row, which leads to a decreasing calculated hardness.

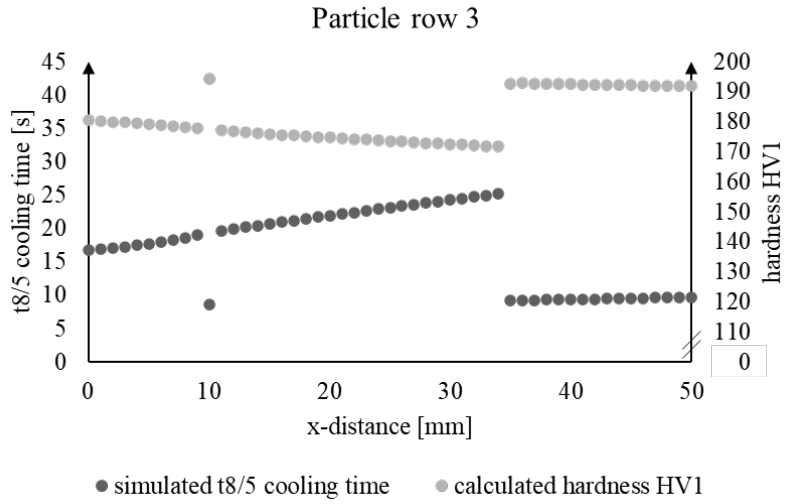

Figure 10. simulated $t_{8/5}$ cooling time and calculated hardness particle row 3

Numerical simulation and experimental values

Experimental results are crucial to ensure the correctness of the numerically generated values. Therefore, welding experiments were performed to generate a cuboid with the boundary conditions stated in Table 2. The welded cuboid can be seen in Figure 12. It was cut vertically in half and then cut horizontally at the 17th welding layer where the numerical results were generated.

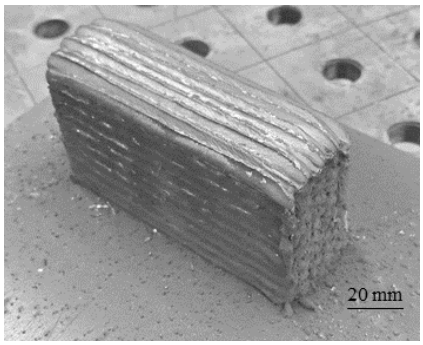

Figure 11. welded cuboid

The hardness regarding the calculated values and the measured values are displayed in Table 3 and in Figure 13 to Figure 15. It is evident that the hardness curve is similar for calculated and measured values for the first and second particle row, but the mean hardness differs for the first particle row (Figure 13) 35.75 HV1, which is 17.76% and for the second particle row (Figure 14) 40.67 HV1 which results in 18.9% difference. The third particle row has a similar curve only to the value in x direction of 35 mm as stated bevor. The mean hardness only differs 26.43 HV1, which is a 12.72% difference. The lower deviation is a result of the jump in $t_{8/5}$ cooling time in the simulation and therefore a jump in hardness closer to the measured values.

Table 3. Comparison measured and calculated hardness

	row 1	**row 2**	**row 3**
Mean value calculated hardness	165,49 HV1	174,55 HV1	181,31 HV1
Mean value measured hardness	201,24 HV1	215,22 HV1	207,74 HV1
Difference absolute	35,75 HV1	40,67 HV1	26,43 HV1
Difference	17,76%	18,90%	12,72%

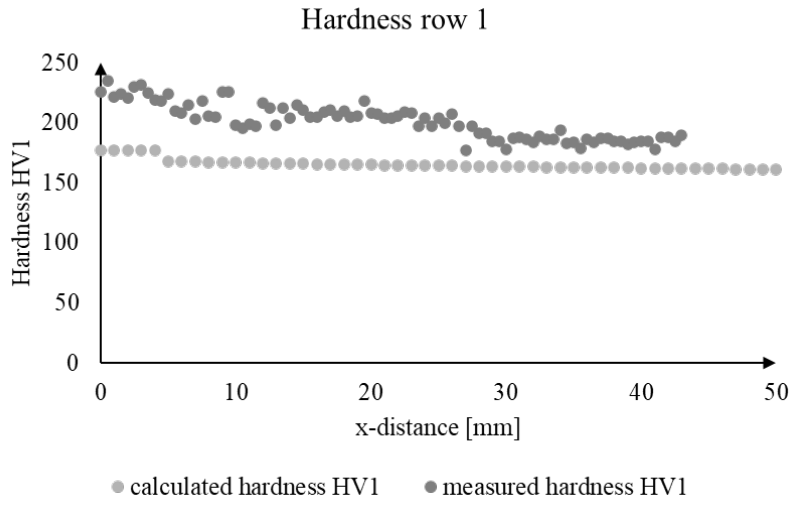

Figure 12. calculated hardness vs measured hardness particle row **1**

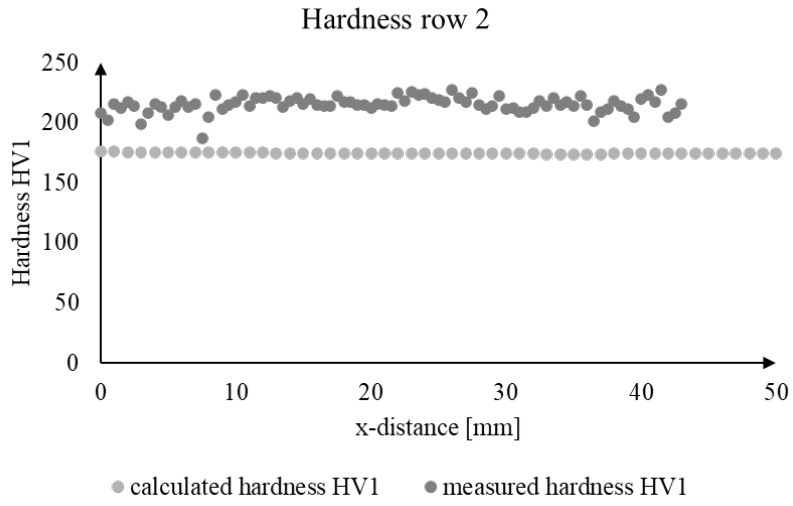

Figure 13. calculated hardness vs measured hardness particle row 2

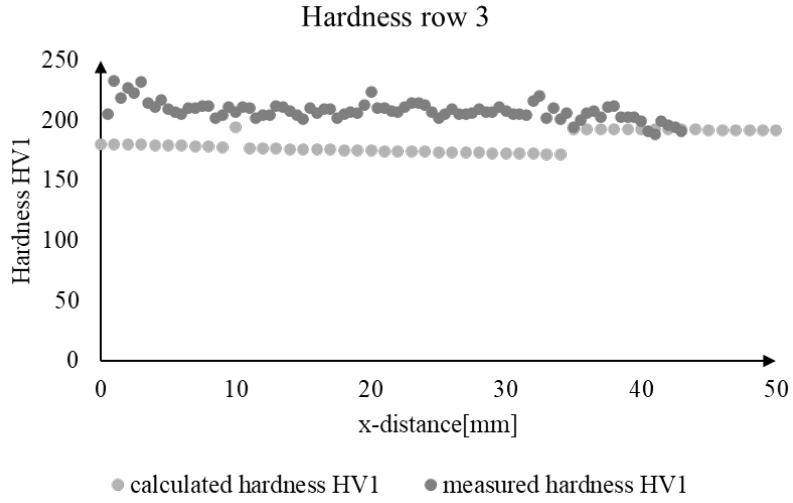

Figure 14. calculated hardness vs measured hardness particle row 3

CONCLUSION AND OUTLOOK

The measured hardness curves at three distinct lines on the cuboid clearly indicate, that the additively manufactured structures using DED-arc are not completely homogenous. The curve of these inhomogeneous hardness values can be replicated using a structural welding simulation to extract the $t_{8/5}$ cooling time to calculate the hardness values. Though the curve is similar, the exact hardness values have a deviation between 12.73% to 18.9% which can be regarded as acceptable deviations considering that relative errors below 20 %, are considered acceptable for a numerical simulation [45]. Thus the numerical welding simulation in combination with regression equations can not only predict the general mechanical properties of additively manufactured wall structures [43] but also for volumes structures. There is generally a higher

relative error for parts as the presented cuboid. In the future the regression equations should be refined using the directly measured hardness values of volume parts in combination with additional thermal imaging to ensure the cooling times are the same as in the simulation. Moreover the simulation might need adjustments in the calibration, due to differences in thermal transfer mechanisms in volume and wall structures [44].

REFERENCES

References

1. https://www.3dprintingmedia.network/wohlers-report-2019-details-striking-range-of-developments-in-am-worldwide. Available online: https://www.3dprintingmedia.network/wohlers-report-2019-details-striking-range-of-developments-in-am-worldwide/ (accessed on 16 June 2021).
2. *DIN 8580:2022-12, Fertigungsverfahren_- Begriffe, Einteilung;* Beuth Verlag GmbH: Berlin.
3. Karunakaran, K.P.; Bernard, A.; Suryakumar, S.; Dembinski, L.; Taillandier, G. Rapid manufacturing of metallic objects. *Rapid Prototyping Journal* **2012**, *18*, 264–280, doi:10.1108/13552541211231644.
4. Hildebrand, J. Additive Fertigung von temperierten Großwerkzeugen mittels Lichtbogen- und Diffusionsschweißtechnik. In *Rapid.Tech + FabCon 3.D*: *International Trade Show + Conference for Additive Manufacturing ; Proceedings of the 15th Rapid.Tech Conference, Erfurt, Germany, 5 – 7 June 2018*; Kynast, M., Eichmann, M., Witt, G., Eds.; Hanser: München, 2018; pp 29–44, ISBN 3446458115.
5. Jahn, S.; Gemse, F.; Broich, U.; Saendig, S. Efficient Diffusion Bonding of Large Scale Parts. *MSF* **2016**, *838-839*, 500–505, doi:10.4028/www.scientific.net/MSF.838-839.500.
6. Karunakaran, K.P.; Suryakumar, S.; Pushpa, V.; Akula, S. Low cost integration of additive and subtractive processes for hybrid layered manufacturing. *Robotics and Computer-Integrated Manufacturing* **2010**, *26*, 490–499, doi:10.1016/j.rcim.2010.03.008.
7. Wu, B.; Pan, Z.; Ding, D.; Cuiuri, D.; Li, H.; Xu, J.; Norrish, J. A review of the wire arc additive manufacturing of metals: properties, defects and quality improvement. *Journal of Manufacturing Processes* **2018**, *35*, 127–139, doi:10.1016/j.jmapro.2018.08.001.
8. Williams, S.W.; Martina, F.; Addison, A.C.; Ding, J.; Pardal, G.; Colegrove, P. Wire + Arc Additive Manufacturing. *Materials Science and Technology* **2016**, *32*, 641–647, doi:10.1179/1743284715Y.0000000073.
9. Ding, D.; Pan, Z.; Cuiuri, D.; Li, H. Wire-feed additive manufacturing of metal components: technologies, developments and future interests. *Int J Adv Manuf Technol* **2015**, *81*, 465–481, doi:10.1007/s00170-015-7077-3.
10. Candel-Ruiz, A.; Kaufmann, S.; Muellerschoen, O. Strategies for high deposition rate additive manufacturing by laser metal deposition. *Lasers in Manufacturing Conference* **2015**, 584.

11. Bergmann, J.P.; Henckell, P.; Ali, Y.; Hildebrand, J.; Reimann, J. *Grundlegende wissenschaftliche Konzepterstellung zu bestehenden Herausforderungen und Perspektiven für die additive Fertigung mit Lichtbogen*: *Studie im Auftrag der Forschungsvereinigung Schweißen und verwandte Verfahren e.V. des DVS;* DVS Media: [Düsseldorf], 2018, ISBN 978-3-96144-038-2.
12. Cunningham, C.R.; Flynn, J.M.; Shokrani, A.; Dhokia, V.; Newman, S.T. Invited review article: Strategies and processes for high quality wire arc additive manufacturing. *Additive Manufacturing* **2018**, *22*, 672–686, doi:10.1016/j.addma.2018.06.020.
13. Mehnen, J.; Ding, J.; Lockett, H.; Kazanas, P. Design study for wire and arc additive manufacture. *IJPD* **2014**, *19*, 2, doi:10.1504/IJPD.2014.060028.
14. Bermingham, M.J.; Nicastro, L.; Kent, D.; Chen, Y.; Dargusch, M.S. Optimising the mechanical properties of Ti-6Al-4V components produced by wire + arc additive manufacturing with post-process heat treatments. *Journal of Alloys and Compounds* **2018**, *753*, 247–255, doi:10.1016/j.jallcom.2018.04.158.
15. Asala, G.; Khan, A.K.; Andersson, J.; Ojo, O.A. Microstructural Analyses of ATI 718Plus® Produced by Wire-ARC Additive Manufacturing Process. *Metall and Mat Trans A* **2017**, *48*, 4211–4228, doi:10.1007/s11661-017-4162-2.
16. Dhinakaran, V.; Ajith, J.; Fathima Yasin Fahmidha, A.; Jagadeesha, T.; Sathish, T.; Stalin, B. Wire Arc Additive Manufacturing (WAAM) process of nickel based superalloys – A review. *Materials Today: Proceedings* **2020**, *21*, 920–925, doi:10.1016/j.matpr.2019.08.159.
17. Lu, X.; Zhou, Y.F.; Xing, X.L.; Shao, L.Y.; Yang, Q.X.; Gao, S.Y. Open-source wire and arc additive manufacturing system: formability, microstructures, and mechanical properties. *Int J Adv Manuf Technol* **2017**, *93*, 2145–2154, doi:10.1007/s00170-017-0636-z.
18. Reimann, J.; Hildebrand, J.; Bergmann, J.P. *3D-Weld - 3D gedruckte Knotenpunkte aus Stahllegierungen für bionische Tragstrukturen;* Fraunhofer IRB Verlag: Stuttgart, 2020, ISBN 9783738804720.
19. Reimann, J.; Henckell, P.; Ali, Y.; Hammer, S.; Rauch, A.; Hildebrand, J.; Bergmann, J.P. Production of Topology-optimised Structural Nodes Using Arc-based, Additive Manufacturing with GMAW Welding Process. *J. Civ. Eng. Constr.* **2021**, *10*, 101–107, doi:10.32732/jcec.2021.10.2.101.
20. Abdelwahab, M.; Tsavdaridis, K.D. Optimised 3D-Printed Metallic Node-Connections for Reticulated Structures. *The 9th International Conference on Steel and Aluminium Structures* **2019**, doi:10.31224/osf.io/jkexd.
21. Galjaard, S.; Hofman, S.; Ren, S. New Opportunities to Optimize Structural Designs in Metal by Using Additive Manufacturing. In *Advances in architectural geometry 2014*; Block, P., Knippers, J., Mitra, N.J., Wang, W., Eds.; Springer: Cham, New York, 2015; pp 79–93, ISBN 978-3-319-11417-0.
22. Gierth, M.; Henckell, P.; Ali, Y.; Scholl, J.; Bergmann, J.P. Wire Arc Additive Manufacturing (WAAM) of Aluminum Alloy AlMg5Mn with Energy-Reduced Gas Metal Arc Welding (GMAW). *Materials (Basel)* **2020**, *13*, doi:10.3390/ma13122671.

23. Gu, J.; Gao, M.; Yang, S.; Bai, J.; Zhai, Y.; Ding, J. Microstructure, defects, and mechanical properties of wire + arc additively manufactured Al Cu4.3-Mg1.5 alloy. *Materials & Design* **2020**, *186*, 108357, doi:10.1016/j.matdes.2019.108357.
24. Ali, Y.; Henckell, P.; Hildebrand, J.; Reimann, J.; Bergmann, J.P.; Barnikol-Oettler, S. Wire arc additive manufacturing of hot work tool steel with CMT process. *Journal of Materials Processing Technology* **2019**, *269*, 109–116, doi:10.1016/j.jmatprotec.2019.01.034.
25. Gordon, J.; Hochhalter, J.; Haden, C.; Harlow, D.G. Enhancement in fatigue performance of metastable austenitic stainless steel through directed energy deposition additive manufacturing. *Materials & Design* **2019**, *168*, 107630, doi:10.1016/j.matdes.2019.107630.
26. Wu, W.; Xue, J.; Wang, L.; Zhang, Z.; Hu, Y.; Dong, C. Forming Process, Microstructure, and Mechanical Properties of Thin-Walled 316L Stainless Steel Using Speed-Cold-Welding Additive Manufacturing. *Metals* **2019**, *9*, 109, doi:10.3390/met9010109.
27. Ghaffari, M.; Vahedi Nemani, A.; Rafieazad, M.; Nasiri, A. Effect of Solidification Defects and HAZ Softening on the Anisotropic Mechanical Properties of a Wire Arc Additive-Manufactured Low-Carbon Low-Alloy Steel Part. *JOM* **2019**, *71*, 4215–4224, doi:10.1007/s11837-019-03773-5.
28. Müller, J.; Grabowski, M.; Müller, C.; Hensel, J.; Unglaub, J.; Thiele, K.; Kloft, H.; Dilger, K. Design and Parameter Identification of Wire and Arc Additively Manufactured (WAAM) Steel Bars for Use in Construction. *Metals* **2019**, *9*, 725, doi:10.3390/met9070725.
29. Rafieazad, M.; Ghaffari, M.; Vahedi Nemani, A.; Nasiri, A. Microstructural evolution and mechanical properties of a low-carbon low-alloy steel produced by wire arc additive manufacturing. *Int J Adv Manuf Technol* **2019**, *105*, 2121–2134, doi:10.1007/s00170-019-04393-8.
30. Feucht, T.; Lange, J.; Waldschmitt, B.; Schudlich, A.-K.; Klein, M.; Oechsner, M. Welding Process for the Additive Manufacturing of Cantilevered Components with the WAAM. In *Advanced Joining Processes*; da Silva, L.F.M., Martins, P.A.F., El-Zein, M.S., Eds.; Springer Singapore: Singapore, 2020; pp 67–78, ISBN 978-981-15-2956-6.
31. Geng, H.; Li, J.; Xiong, J.; Lin, X. Optimisation of interpass temperature and heat input for wire and arc additive manufacturing 5A06 aluminium alloy. *Science and Technology of Welding and Joining* **2017**, *22*, 472–483, doi:10.1080/13621718.2016.1259031.
32. Zhao, Y.; Jia, Y.; Chen, S.; Shi, J.; Li, F. Process planning strategy for wire-arc additive manufacturing: Thermal behavior considerations. *Additive Manufacturing* **2020**, *32*, 100935, doi:10.1016/j.addma.2019.100935.
33. Montevecchi, F.; Venturini, G.; Scippa, A.; Campatelli, G. Finite Element Modelling of Wire-arc-additive-manufacturing Process. *Procedia CIRP* **2016**, *55*, 109–114, doi:10.1016/j.procir.2016.08.024.
34. Ding, J.; Colegrove, P.; Mehnen, J.; Ganguly, S.; Sequeira Almeida, P.M.; Wang, F.; Williams, S. Thermo-mechanical analysis of Wire and Arc Additive Layer Manufacturing process on large multi-layer parts. *Computational Materials Science* **2011**, doi:10.1016/j.commatsci.2011.06.023.

35. Graf, M.; Pradjadhiana, K.P.; Hälsig, A.; Manurung, Y.H.P.; Awiszus, B. Numerical simulation of metallic wire arc additive manufacturing (WAAM). In . Proceedings of the 21st International ESAFORM Conference on Material Forming: ESAFORM 2018, Palermo, Italy, 23–25 April 2018; Author(s), 2018; p 140010.
36. Graf, M.; Hälsig, A.; Höfer, K.; Awiszus, B.; Mayr, P. Thermo-Mechanical Modelling of Wire-Arc Additive Manufacturing (WAAM) of Semi-Finished Products. *Metals* **2018**, *8*, 1009, doi:10.3390/met8121009.
37. Hu, Z.; Qin, X.; Shao, T. Welding Thermal Simulation and Metallurgical Characteristics Analysis in WAAM for 5CrNiMo Hot Forging Die Remanufacturing. *Procedia Engineering* **2017**, *207*, 2203–2208, doi:10.1016/j.proeng.2017.10.982.
38. Montevecchi, F.; Venturini, G.; Grossi, N.; Scippa, A.; Campatelli, G. Heat accumulation prevention in Wire-Arc-Additive-Manufacturing using air jet impingement. *Manufacturing Letters* **2018**, *17*, 14–18, doi:10.1016/j.mfglet.2018.06.004.
39. Ding, J. Thermo-mechanical analysis of wire and arc additive manufacturing process; Cranfield University.
40. Pu, X.; Zhang, C.; Li, S.; Deng, D. Simulating welding residual stress and deformation in a multi-pass butt-welded joint considering balance between computing time and prediction accuracy. *Int J Adv Manuf Technol* **2017**, *93*, 2215–2226, doi:10.1007/s00170-017-0691-5.
41. Salzgitter Flachstahl GmbH. S355J2+N: Unlegierte Baustähle. Available online: https://www.salzgitter-flachstahl.de/fileadmin/mediadb/szfg/informationsmaterial/produktinformationen/warmgewalzte_produkte/deu/S355J2_N.pdf (accessed on 17 July 2021).
42. Westfälische Drahtindustrie GmbH. Schweisstechnik: High Quality Welding Wire. Technisches Handbuch. Available online: https://www.wdi.de/fileadmin/user_upload/WDI_SFHandbuch_3_Edition_screen.pdf (accessed on 12 July 2021).
43. Reimann, J.; Hammer, S.; Henckell, P.; Rohe, M.; Ali, Y.; Rauch, A.; Hildebrand, J.; Bergmann, J.P. Directed Energy Deposition-Arc (DED-Arc) and Numerical Welding Simulation as a Hybrid Data Source for Future Machine Learning Applications. *Applied Sciences* **2021**, *11*, 7075, doi:10.3390/app11157075.
44. Henckell, P.; Gierth, M.; Ali, Y.; Reimann, J.; Bergmann, J.P. Reduction of Energy Input in Wire Arc Additive Manufacturing (WAAM) with Gas Metal Arc Welding (GMAW). *Materials (Basel)* **2020**, *13*, doi:10.3390/ma13112491.
45. Prajadhiama, K.P.; Manurung, Y.H.P.; Minggu, Z.; Pengadau, F.H.S.; Graf, M.; Haelsig, A.; Adams, T.-E.; Choo, H.L. Development of Bead Modelling for Distortion Analysis Induced by Wire Arc Additive Manufacturing using FEM and Experiment. *MATEC Web Conf.* **2019**, *269*, 5003, doi:10.1051/matecconf/201926905003.

CONTACS

Jan Reimann email: jan.reimann@tu-ilmenau.de
ORCID: https://orcid.org/0000-0001-6995-752X

